Research Article

Spatial Fluctuating Pressure Calculation of Underwater Counter Rotating Propellers under Noncavitating Condition

L. X. Hou [iD] **and A. K. Hu**

School of Naval Architecture and Ocean Engineering, Dalian Maritime University, No. 1 Linghai Street,
Ganjingzi District, Dalian, Liaoning 116026, China

Correspondence should be addressed to L. X. Hou; 07093129@163.com

The spatial fluctuating pressure field (FPF) of counter rotating propeller (CRP) under noncavitating condition is investigated. The hydrodynamic performance and pressure distributions on the blade surfaces are obtained through low-order potential-based panel method, which is also used to analyze the hydrodynamic interaction between the front and rear propellers of CRP as well as the hydrodynamic interference between any solid surface and propeller. The interaction between the given solid spherical surface and propeller is used to simulate the spatial FPF of propeller, and the fluctuating pressure induced by a propeller over one revolution is analyzed in frequency domain through fast Fourier transform. The method proposed is validated through two given propellers by comparing the calculation results with test data. The FPFs of the front and rear propellers are calculated and compared with that of the corresponding single propeller. The result shows that the CRP produces weaker FPF compared with the single propeller.

1. Introduction

Working in the nonuniform wake field behind ship hull, the propeller is subjected to unsteady surface loadings which lead to fluctuating pressure. It is well known that the fluctuating pressure can cause serious vibration problem on ship hull as well as the appendages behind the vessel. The fluctuating pressure induced by marine propeller can be classified into cavitation and noncavitation fluctuating pressure. The marine propeller cavitation is the most prevalent source of underwater fluctuating pressure in ocean. To the authors' knowledge, a lot of work has been done on the fluctuating pressure analysis of marine propeller under cavitation condition. Breslin et al. [1] studied propeller-induced hull pressures arising from intermittent blade cavitation, loading, and thickness using theoretical method coupled with experiments. Numerical methods have been developed based on surface panel method to compute the fluctuating pressure of cavitating propellers and compared the computational results with experimental data [2]. Seol [3] and Berger et al. [4] addressed the pressure fluctuation induced by a propeller sheet cavitation. The developed time domain

prediction methods provided reasonable results, and these results are in good agreement with the experimental results. Kanemaru and Ando [5] simulated unsteady sheet cavitation patterns, cavity volume evolution, and pressure fluctuations around marine propellers in nonuniform wake using the simple surface panel method SQCM with consideration of viscous effects to improve the calculation accuracy. The CFD technology has been widely used to predict the fluctuating pressure generated by cavitating propeller. Kawamura and Kiyokawa [6] simulated cavitating flows around a propeller rotating in a ship wake. Their results demonstrated that the magnitude of the pressure fluctuations increased greatly during cavitation, though the pressure fluctuations associated with the cavitation were still underestimated and the higher frequency components were not reproduced. Sato et al. [7] predicted the sheet cavitation behavior and pressure fluctuations using CFD software. Their simulations accurately predicted the 1st blade frequency component of the pressure fluctuations, while the high frequency components were severely underestimated due to the inability to simulate the tip vortex cavitation. Ji et al. [8] verified that the acceleration due to the cavity volume changes was the main source of

the pressure fluctuations excited by the propeller cavitation by adopting the CFD technique. Lloyd et al. [9] calculated the pressure pulses inside the cavitation tunnel using the computational fluid dynamics code ReFRSCO. In order to predict the pressure pulse, Peralli et al. [10] investigated the wetted and cavitating flow around the INSEAN E779A propeller in a cavitation tunnel using the uRANS and BEM-BEM, respectively, and discussed the pro and cons of these two methods. Bensow and Gustafsson [11] investigated how hull forces and pressure are influenced by small propeller tip clearance by creating a setup where systematic variation of tip clearance could be achieved at similar propeller conditions. The simulations were performed using a scale resolved PANS approach combined with cavitation modelling considering the fluid as a mixture and incorporating mass transfer source terms.

However, submarines and torpedoes are usually operated deep enough under the sea to avoid cavitation [12], and some low speed vessels do not have noticeable cavitation phenomenon. It is of great significance to have investigations about the fluctuating pressure generated by marine propeller under noncavitating condition. Early researches about fluctuating pressure generated by propeller under noncavitating condition mainly obtained some empirical formulas according to a large quantity of accumulated data. Garguet and Lepeix [13], Tsakonas et al. [14], and Hu et al. [15] considered the influences of the hull and the free surface by introducing solid wall correction factor. Chen and Zhou [16] calculated the noncavitating fluctuating pressure of propeller in given wake field through CFD software. Güngör and Bedii Özdemir [17] investigated the performance of an inclined propeller in both noncavitating and cavitating conditions using a finite volume based solver and compared the results with the experimental data. The sliding mesh technique was used to implement the rotations in URANS solver with the renormalization group (RNG) k-ε turbulent model. In the noncavitating case, the amplitudes of the pressure fluctuations were in agreement with the experimental data, but those of pressure pulses in the cavitating condition were underpredicted.

As the world's energy shortage problem gets increasingly serious and the energy efficiency design index (EEDI) for new ship came into effect on January 1, 2013, reducing fuel consumption and building green ship not only relate directly to the operating costs but also help to deal with other risk factors [18]. As the power source of ships, efficient propulsion machinery will reduce fuel consumption and operation costs. The application of the counter rotating propeller (CRP) has been developed significantly in last decades. Compared with single propeller, both of the front and rear propellers of CRP have lower loadings while supplying the same thrust as the single propeller. Therefore, the CRP has better cavitation performance under the same operating condition. Thus, it is significant to investigate the noncavitation fluctuating pressure of CRP theoretically. Nowadays, works concerning the fluctuating pressure field of CRP are hard to find.

In the present paper, the spatial FPF of CRP under noncavitating condition is investigated in detail. The low-order potential based panel method is adopted throughout this study, and the computation formulas for fluctuating pressure prediction are proposed. The calculation program based surface panel method is validated by comparing the calculation results and test data of DTRC P4118. Two given single propellers' fluctuating pressures are calculated and the results are compared with the test data to validate the fluctuating pressure prediction method. Then the FPFs of a set of CRP and the corresponding single propeller are calculated. The hydrodynamic interaction between the front and rear propellers of CRP is considered. Through analysis, the FPF characteristics of CRP can be obtained, which will provide a basis for proper stern vibration control strategies under noncavitating condition.

2. Methods

The panel method has been proved to be effective for hydrodynamic performance prediction of propeller [19]. Studies by Hsin [20] and Kinnas and Fine [21] have given specific description about the details and fundamentals of panel method. Thus, this paper only gives a brief description. This method derived from Green's theorem and the velocity potential ϕ_p at a fixed point p located anywhere in the flow field can be expressed as follows:

$$4\pi\varsigma\phi_p = \int_S \left[\phi_q \frac{\partial G}{\partial n} - G \frac{\partial \phi_q}{\partial n} \right] dS + \int_{S_W} \Delta\phi \frac{\partial G}{\partial n} dS, \quad (1)$$

where S, S_w represent the propeller surface and the wake surface respectively, $\Delta\varphi$ is the potential jump across the wake sheet, ϕ_q represents the velocity potential at any point q on S, and G denotes Green's function. In the case of unbounded three-dimensional fluid domain, G is given as

$$G = G(p;q) = \frac{1}{R(p;q)} \quad (2)$$

with $R(p;q)$ being the distance between points p and q. ς in (1) has values as follows:

(i) $\varsigma = 1$, if p lies in the flow field, but not on S.

(ii) $\varsigma = 1/2$, if p lies on S.

(iii) $\varsigma = 0$, if p lies outside S.

The propeller surface and wake sheet are discretized with hyperboloidal panels. A constant source and a constant dipole are then distributed on each panel. During unsteady calculation, the integral equation (1) is solved at each time step, and time-dependent terms are updated at the next time step. The specific unsteady treatment is given in literature [20]. The time domain is discretized into equal time intervals Δt, and (1) at each time step $n = t/\Delta t$ can be discretized as follows:

$$\sum_{j=1}^{N_P} a_{i,j}\phi_j(n) + \sum_{m=1}^{N_R} W_{i,m,1}\Delta\phi_{m,1}(n) = \text{RHS}_i(n),$$

$$i = 1, 2, \ldots, N_P,$$

$\text{RHS}_i\,(n)$

$$
\begin{aligned}
= &\sum_{Z=1}^{N_B}\sum_{j=1}^{N_P} b_{i,j}^Z \sigma_j^Z\,(n) - \sum_{Z=2}^{N_B}\sum_{j=1}^{N_P} a_{i,j}^Z \phi_j^Z\,(n) \\
&- \sum_{Z=2}^{N_B}\sum_{m=1}^{N_R}\sum_{l=1}^{N_W} W_{i,m,l}^Z \Delta\phi_{m,l}^Z\,(n) \\
&- \sum_{m=1}^{N_R}\sum_{l=2}^{N_W} W_{i,m,l}^Z \Delta\phi_{m,l}\,(n),
\end{aligned}
$$

$$(3)$$

where N_B is the number of blades. For each blade, N_C is the number of chordwise panels, N_R is the number of spanwise panels, $N_P = 2 \times N_C \times N_R$ is the total number of panels, and N_W is the number of chordwise panels in the wake. The influence coefficients $a_{i,j}^Z$ and $b_{i,j}^Z$ are defined as the potentials induced at panel i by unit (constant) strength dipole and source distributions, respectively, located at panel j on blade Z. The wake influence coefficients $W_{i,m,l}^Z$ are defined similarly. The definitions of the influence coefficients are given in the dissertation of Hsin [20].

As the propeller hub is nonlifting, the dipoles on the panels of hub are set to zero, so just a constant source is distributed on each panel of hub. Once the velocity potential is determined, the velocities on the propeller surfaces can be obtained by differentiating the resulting velocity potential. Then the pressure distribution is calculated through Bernoulli's equation.

In this paper, the solid surface S is used for spatial fluctuating pressure field analysis of propeller. The local intensity of the distribution is denoted by $\sigma(q)$, where the source point q now denotes a general point of the surface S, and then the normal velocity boundary condition must be satisfied at any point p on the surface S

$$
2\pi\sigma\,(p) + \iint_S \sigma\,(q)\,\frac{\partial}{\partial n}\frac{1}{r\,(p,q)}\,dS\,(q) = -v_{tp}\cdot n_p,
$$
$$
v_{tp} = V_0 + v_{inp},
$$

$$(4)$$

where $r(p,q)$ is the distance between p and q, v_{tp} is the inflow velocity of point p, v_{inp} is the velocity induced by the propeller at point p, and can be obtained through panel method.

As the solid surface just has source distribution, the velocity induced by the solid surface at any point d on the propeller surface can be expressed as follows:

$$
v_d = \frac{1}{4\pi}\iint_S \sigma\,(q)\,\nabla\left(\frac{1}{R\,(d,q)}\right) dS\,(q),
$$

$$(5)$$

where $R(d,q)$ is the distance between d and q.

The solid surface is divided into a number of quadrilateral source panels; the dimensions of which are small in comparison with the surface. The solution is constructed in terms of the source strengths on the surface. The integral equation for the source strengths is approximated by a matrix equation on the assumption of uniform strength on each panel. Equations (4)~(5) can be discretized as follows:

$$
2\pi\sigma_i + \sum_{j=1}^{N_0}\sigma_j \iint_{s_j}\frac{\partial}{\partial n_i}\frac{1}{r_{ij}}\,ds = -v_{ti}\cdot n_i \quad i = 1,\ldots,N_0,
$$

$$(6)$$

$$
v_{ti} = V_0 + v_{ini},
$$

$$(7)$$

$$
v_d = \frac{1}{4\pi}\cdot\sum_{j=1}^{N_0}\sigma_j \iint_{s_j}\nabla\left(\frac{1}{R_j}\right) ds.
$$

$$(8)$$

Here, N_0 is the panel number of the solid surfaces, v_{ti} is the inflow velocity of the ith panel, and v_{ini} is the velocity induced by the propeller on the ith panel of the solid surface. For (6), the second term is zero when the jth and ith panels are on the same plane; namely, $\sigma_i = -v_{ti}\cdot n_i/2\pi$. R_j is the distance between the point d and the jth panel of the solid surface.

The velocity induced by the solid surface on the propeller surface can be obtained through (8). By adding the velocities induced by the solid surface to the inflow velocities the unsteady hydrodynamic performance of the propeller as well as the velocities induced by the propeller on the solid surface panels are recalculated. Solving (6) can get new source strength σ_i. Through this iterative calculation, the stable source strengths and velocities on the panels of the solid surface can be obtained at each time step. The pressure distribution on the solid surface is obtained through Bernoulli's equation. The hydrodynamic performance coefficients can be defined as follows:

$$
J = \frac{V_0}{nD};
$$
$$
K_T = \frac{T}{\rho n^2 D^4};
$$
$$
K_Q = \frac{Q}{\rho n^2 D^5},
$$

$$(9)$$

where J is the advance coefficient, ρ is the ambient fluid density, n and D, respectively, denote the rotational speed and the diameter of the propeller, V_0 is the ship speed, T and Q are the thrust and torque of the propeller, and K_T and K_Q are the thrust and torque coefficients of propeller, respectively.

As the propeller works in the nonuniform flow field, the pressure on the solid surface changes periodically. The Fourier transform is adopted to transform the pressure signals from the time domain to frequency domain, and the fluctuating pressure coefficient can be obtained:

$$
K_{Pn} = \frac{P_n}{\rho n^2 D^2} \quad n = 1, 2, 3, \ldots,
$$

$$(10)$$

where P_n is the nth blade frequency harmonic component of the fluctuating pressure (zero to peak) and K_{Pn} represents the fluctuating pressure coefficient of the nth blade frequency harmonic component.

3. Method Validation

The surface panel method proposed in this paper is applied to the propeller DTRC 4118 whose specific parameters are given
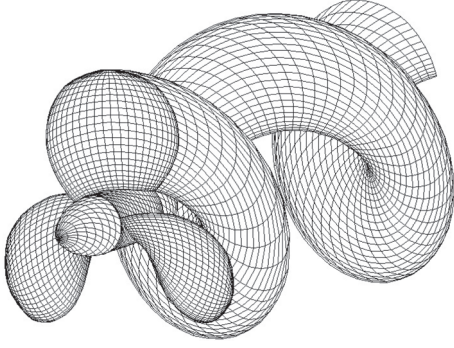
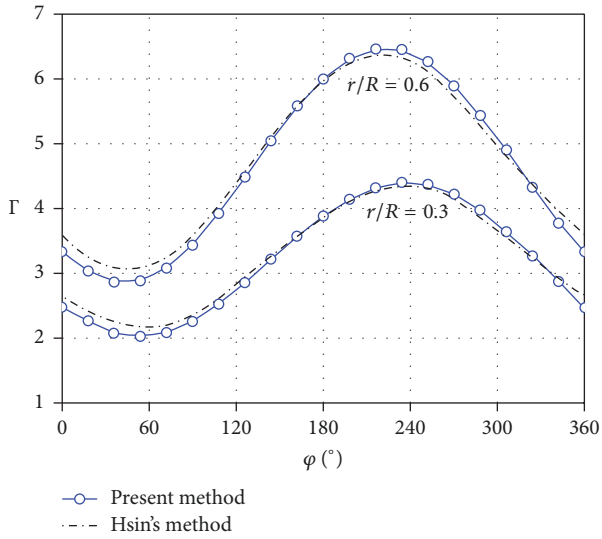FIGURE 1: Panel arrangement of DTRC 4118 propeller.

TABLE 1: Main parameters of the propeller.

Title	1st model	2nd model
Model diameter (D_m)	0.24 m	0.24 m
Number of blades (Z)	6	6
Expanded blade area ratio (Exar)	0.683	0.81
Pitch ratio$_{(mean)}$	1.039	1.043
Skew	32°	32°
Direction of rotation	Right-handed	Right-handed

FIGURE 2: Comparison with Hsin's method.

by Hsin [20]. The panel arrangements of propeller model and slipstream of the key blade are illustrated in Figure 1. The cosine spacing is employed in the chordwise direction and spanwise direction of the propeller blade. The calculation accuracy will be much satisfying when the propeller blades are discretized using more than 14 chordwise panels and 14 spanwise panels [19]. The panel number of the propellers studied in this paper is much more than 14×14, and the calculation accuracy can be ensured. What is more, the slipstream model is linear. The linear slipstream model can satisfy the calculation accuracy required well [22] and is also used for other calculations of this paper. The incoming wake is assumed to be axial, with a once per revolution circumferential variation:

$$U_{Sx} = V_0 \left(1 + u_g \cos\theta_S\right) \tag{11}$$

with u_g being the amplitude of the wake variation, taken equal to 0.2. The advance coefficient is 0.833, and the propeller is operated at 120 rpm with a forward velocity of 1.6 m/s. The density of the undisturbed medium of standard water is 1026 kg/m^3. In order to validate the panel method given in this paper, the calculation results are compared with the results of Hsin. The comparison results are shown in Figure 2,

which gives the circulation distributions versus blade angle at two propeller radiuses; namely, $r/R = 0.3$ and $r/R = 0.6$. It can be known that the calculation results show excellent agreement with the results of Hsin.

The method proposed in this paper is validated by comparing the theoretical calculation results with the experiment values of two containership propellers. The main parameters of two propellers studied in this paper are shown in Table 1. Figure 3 gives the propeller models used in tests.

The tests were carried out in the cavitation tunnel laboratory of Shanghai Ship & Shipping Research Institute (SSSRI). The pressure fluctuation signals were amplified by the amplifier YD-28 and stored by the wave profile storage. Then the sampled signals were input into computer for fast Fourier transform (FFT) processing. The wake field used for both of propellers is given in Figure 4, the in-plane wake velocities are not considered.

The pressure fluctuation survey was arranged at five measuring points. Five pressure sensors were installed in a plate right above propeller model. The distance between the plate and center line of propeller shaft was 0.188 m (model radius 0.12 m plus tip clearance 0.068 m) in this case. Figure 5 gives the outline of this arrangement.

In the tests, the thrust coefficient was kept the same with that of full scale condition. The thrust coefficient of the first propeller is 0.2079 and that of the second propeller is 0.2231. The rotational speeds of both of propellers were kept fixed to a value of $n = 21.48$ rps throughout the tests. The advance speeds in tests were set to satisfy the required thrusts in the given wake field. The results of pressure fluctuation measurement are presented in form of pressure fluctuating coefficient K_{Pn}. For theoretical calculation, the coordinate is denoted by (X, Y, Z), a right-handed system with the X-axis pointing downstream along the propeller axis; the coordinate origin is located at the center of the propeller disk. The Y-axis points to starboard and Z-axis upward. Figure 6 gives the panel distributions of the 1st propeller surface and a plate large enough as well as the slipstream of the key blade. The 2nd propeller has the same panel distributions. The theoretical calculations adopt the same operating conditions with the model experiments. Table 2 gives the time-averaged hydrodynamic performance coefficients over one revolution. It can be known that the calculation results are in good agreement with the experiment data and that the errors are in acceptable scope.

(a)

(b)

FIGURE 3: Propeller models for experiments: (a) 1st propeller model. (b) 2nd propeller model.

TABLE 2: Time-averaged results of hydrodynamic performance.

	K_T-cal	K_T-exp	K_T-error	$10K_Q$-cal	$10K_Q$-exp	K_Q-error
1st propeller	0.2125	0.2079	2.23%	0.3624	0.3506	3.37%
2nd propeller	0.2279	0.2231	2.18%	0.3786	0.3643	3.93%
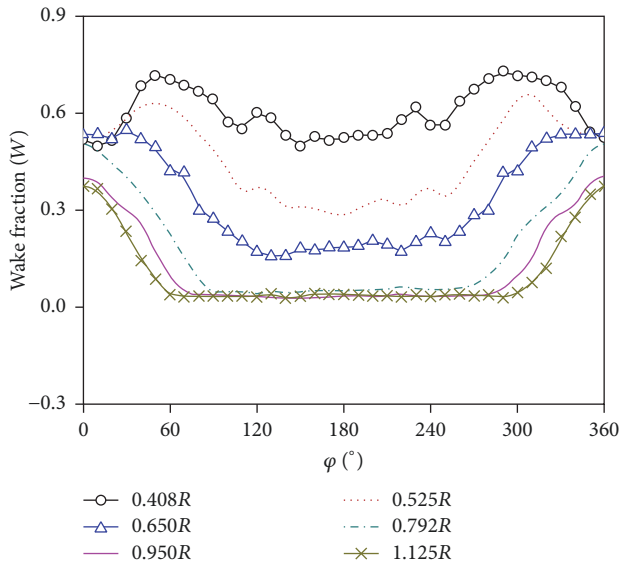
FIGURE 4: Simulated axial wake contours.

FIGURE 5: Arrangement of sensors for measuring pressure fluctuation.

Figures 7 and 8 give the comparisons between the experiment values and the calculation results of the fluctuating pressure coefficients of the first four blade frequency harmonic components. It can be known that the calculation results are slightly less than the experiment values as a whole; this is mainly because cavitation can not be avoided totally during the experiment in the cavitation tunnel but not be prominent. What is more, somewhat difference exists between the theoretical model and the experimental arrangement. Nev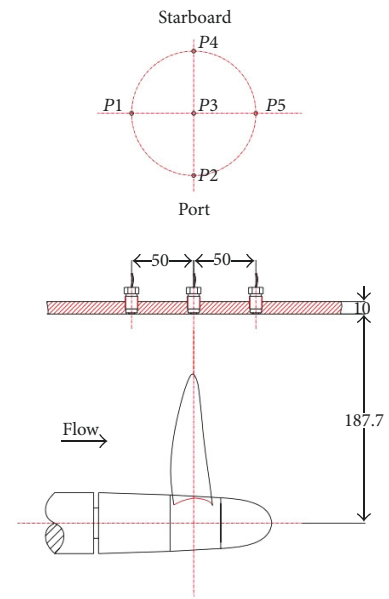ertheless, the result shows that the calculation results agree with the experiment values well and provides a satisfying verification of the theory proposed in this paper.

4. Calculation Results

4.1. Hydrodynamic Performance Prediction. Taking a container ship as the research object, the wake field of the model scale vessel at the propeller plane measured in water tank is shown in Figure 9. The counter rotating propeller HEU96
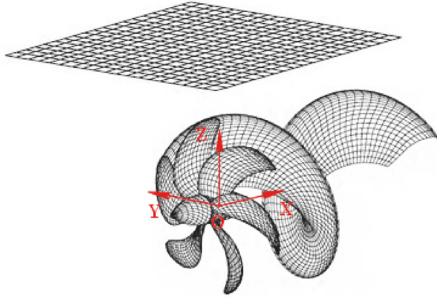
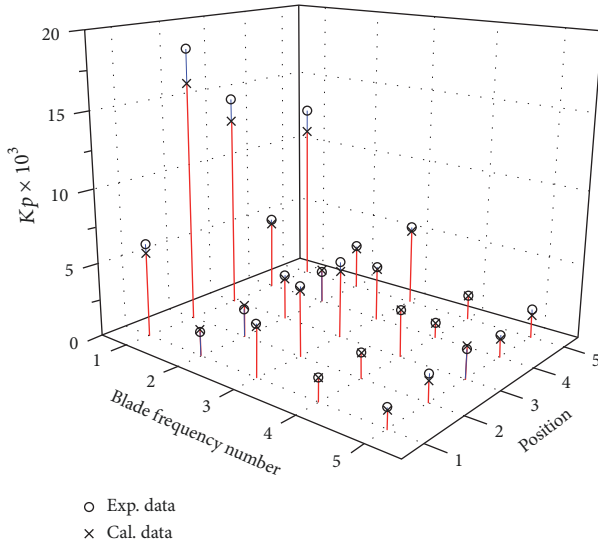FIGURE 6: Propeller and plate for verification.

FIGURE 9: Wake field at propeller plane.

○ Exp. data
× Cal. data

FIGURE 7: Comparisons between the experiment values and calculation results of 1st propeller.

○ Exp. data
× Cal. data
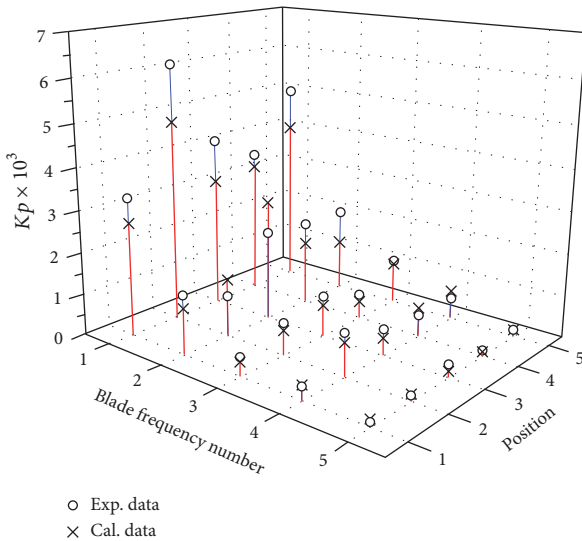
FIGURE 8: Comparisons between the experiment values and calculation results of 2nd propeller.
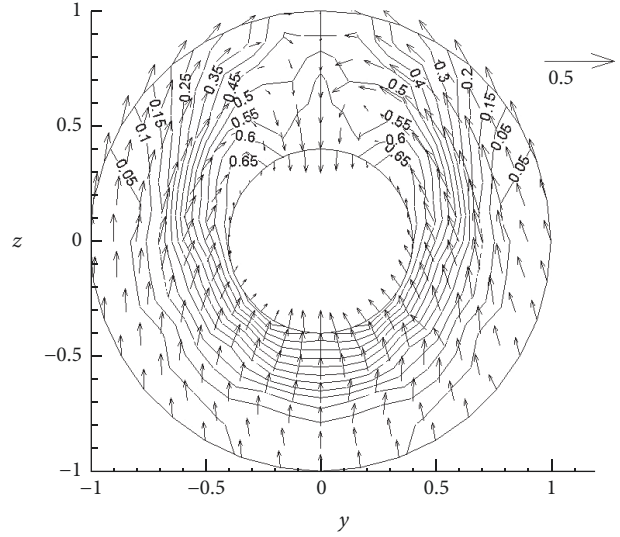
CRP and the corresponding single propeller HEU96 propeller studied in this paper are designed by Harbin Engineering University. The 5-bladed HEU96 propeller operates at 8.77 rps with a forward velocity of 1.6 m/s. The front and rear propellers of HEU96 CRP have 4 and 5 blades, respectively, and the front propeller is a right-handed propeller and rear one left-handed. Compared with the single propeller the CRP can have an increase in propulsive efficiency by 12.09%. The CRP has the same advance coefficient and forward velocity with the single propeller. The interference between the front and rear propellers is considered through induced velocities during the calculation iteration.

This paper has unsteady hydrodynamic performance predictions of CRP and single propeller, respectively, and the unsteady hydrodynamic performance of CRP is predicted considering the interactions between the front and rear propellers. As the rear propeller works in the slipstream of forward propeller, the influence coefficients of the slipstream of forward propeller may have singularity when the panel centroids of slipstream get too close to those of rear propeller. It is assumed that the singular influence coefficient appears when the distance between two panel centroids is less than one hundredth of the length of relevant propeller panel diagonal. This paper ignores the singular influence coefficients of slipstream directly as skimming individual singular influence coefficient has little effect on the hydrodynamic performance calculation [22].

Figures 10 and 11 give the thrust and torque coefficients over one revolution. The thrust and torque coefficients of the front and rear propellers of CRP are defined based on the single propeller parameters. The CRP produces roughly the same thrust with the single propeller, whereas the torque of CRP is obviously smaller than that of the single propeller. Therefore, the CRP can raise the propulsive efficiency significantly compared with the single propeller. Both the thrust and the torque show significant periodicities. The fluctuations
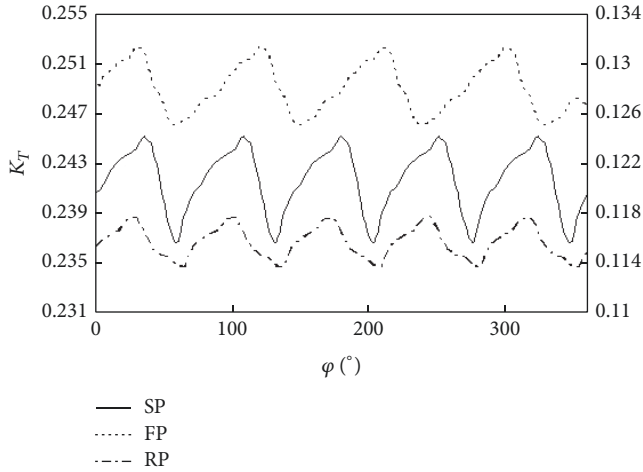
FIGURE 10: Thrusts over one revolution for single propeller (SP) and CRP (FP: front propeller, RP: rear propeller).
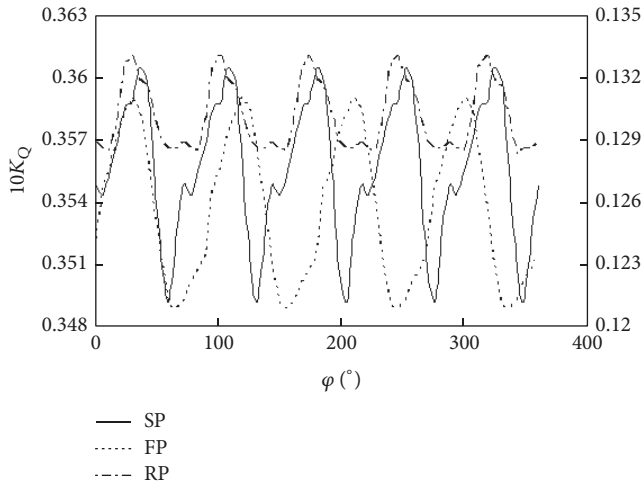

FIGURE 11: Torques over one revolution for single propeller (SP) and CRP (FP: front propeller, RP: rear propeller).

in thrust and torque of front and rear propellers of CRP are somewhat smaller compared with the single propeller.

As the rear propeller blades run through the slipstream of the front propeller, the front propeller has strong influence on the rear propeller and makes the inflow velocities of the rear propeller more circumferentially uniform compared with the wake velocities behind the ship hull. Therefore, the oscillation amplitudes of the thrust and torque of the rear propeller are smaller compared with those of the front propeller, especially; the fluctuation of rear propeller torque is evened out obviously. As the influence of the rear propeller on the front propeller is weak the oscillation amplitudes of the thrust and torque of the front propeller are not improved significantly but still less than those of the single propeller due to lower blade loading.

As the FPF of propeller is closely related to unsteady hydrodynamic forces, the CRP can have better fluctuating pressure performance.

4.2. FPF Calculation. In order to calculate and analyze the spatial FPF of CRP, the spherical surfaces of CRP and the corresponding single propeller are constructed, as shown in Figure 12. The Cartesian coordinate (X, Y, Z) is used, and X points in the downstream direction, Y starboard, and Z upstream direction. The center of the spherical surface is located at the midpoint between the front and rear propeller plane centers. The diameter D_s of spherical surface of CRP is 3.5 times the front propeller diameter. The diameter of the spherical surface for the single propeller is the same as that of the CRP, and the center of the spherical surface is located at the single propeller disk center. We assume that the existence of spherical surface has no effect on the initial inflow velocity of propulsor.

For the single propeller, the FPF calculation is clear and simple. However, the analysis about the FPF of CRP is complex owing to the complicated construction of CRP. For better understanding about the calculation process of the FPF of CRP, Figure 13 gives the iterative process of FPF calculation of CRP. In Step 1 of Figure 13, the induced velocities from rear propeller and spherical surface are not considered for the performance prediction of forward propeller in the first iterative process. In Step 3, the induced velocities from the spherical surface are not considered for the performance prediction of the rear propeller in the first iterative process. In Steps 2 and 4, the induced velocities from the forward propeller and the rear propeller are calculated at each time step during unsteady hydrodynamic performance predictions. Since the relative positions of the forward propeller, rear propellers, and the spherical surface are specified at any time step, the induced velocities between the forward propeller and rear propeller as well as those of the forward and rear propellers at the panel centroids of spherical surface are calculated at each time step. In Step 7, the induced velocities of the spherical surface at the panel centroids of the forward and rear propellers are calculated at each time step. In Step 6, the forces of system refer to the total thrust and the total torque of the forward and rear propellers. Once the total velocities on the spherical surface are determined, the pressure can be calculated through Bernoulli's equation, and the fluctuating pressure induced by the forward and rear propellers can be obtained.

Comparing with the hydrodynamic performance calculations of CRP in Section 4.1, the FPF calculations of CRP need more computation as the interferences between the spherical surface and propellers are considered. The FPF calculations of CRP converge after 8 loop iterations, while the convergence results of hydrodynamic forces given in Figures 10 and 11 just need 5 iterations.

During the calculations, the influence coefficients of the slipstream of propeller may have singularity when the panel centroid of slipstream gets too close to that of spherical surfaces. The singular influence coefficients are also ignored. The calculated three-dimensional FPFs of the single propeller and CRP are shown in Figures 14, 15, and 16. For the sake of constructive analysis, the front hemispherical surfaces are translated 5 times the front propeller diameter along the negative X direction and the rear hemispherical surfaces are translated the same distance along the positive X direction,

(a)   (b)
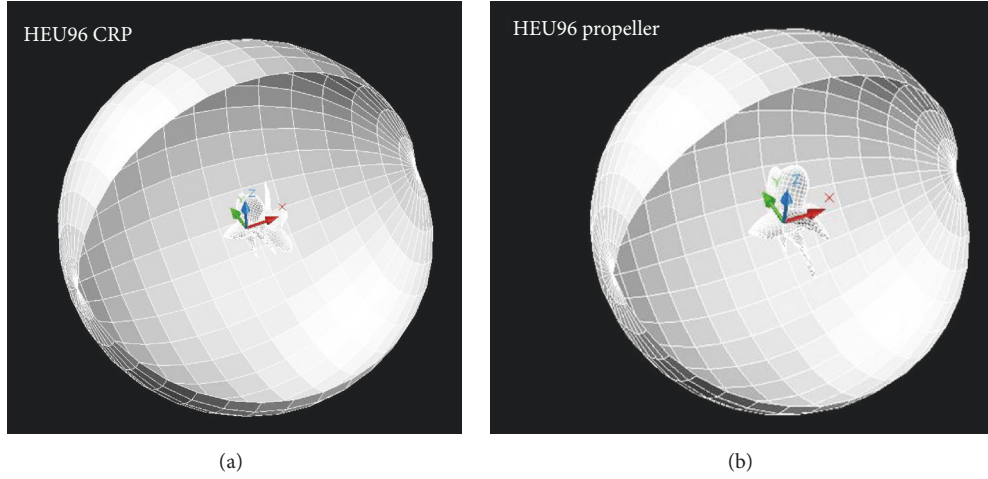
FIGURE 12: Spherical surfaces for calculation: (a) CRP spherical surface system and (b) single propeller spherical surface system.
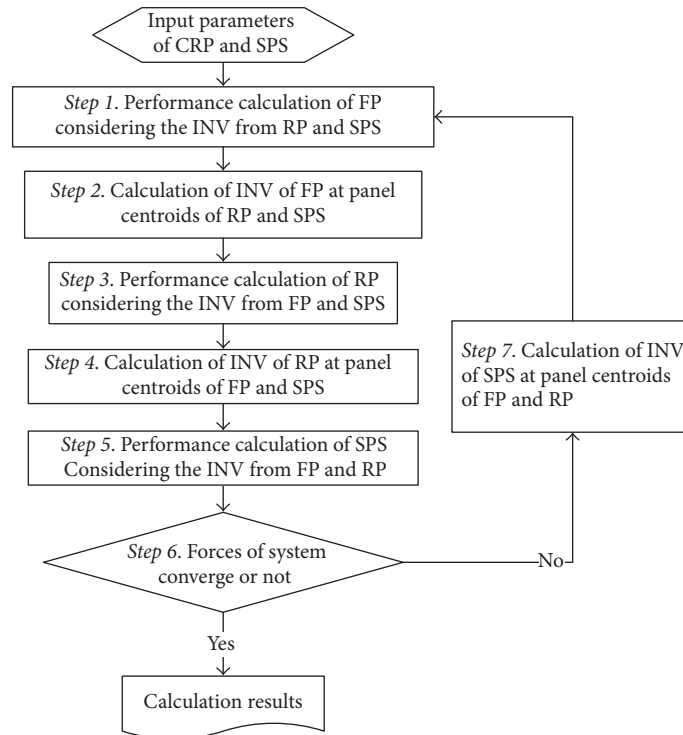

FIGURE 13: Iteration flow diagram of FPF calculations of CRP. INV is the abbreviation of induced velocities. FP and RP represent the forward and rear propellers, and SPS denotes the spherical surface.

and the positions of propellers remain unchanged. Since the single propeller and CRP have different diameters, the fluctuating pressure coefficients of the front and rear propellers of CRP are defined based on the diameter and rotational speed of the single propeller. It can be known from Section 3 that the fluctuating pressure coefficient K_{Pn} decreases rapidly with the increase of blade passage frequency (BPF); thus the first-order fluctuating pressure coefficient K_{P1} is given here.

It can be seen from Figure 14 that the single propeller has strong fluctuating pressure distribution on the solid spherical surface within the longitudinal cylinder of propeller. In other words, the fluctuating pressure induced by the single propeller is obvious ahead of the propeller and within the slipstream. The rotating blades make strong disturbance in the slipstream by inducing a swirling motion of the water. In addition, the suction role of propellers can induce obvious fluctuating pressure. We can know from further analysis about Figure 14 that the FPF at the port side is significantly stronger than that at the starboard. This is mainly because the propeller has stronger disturbance at the port side. What is more, the fluctuating pressure near the propeller plane is weak.
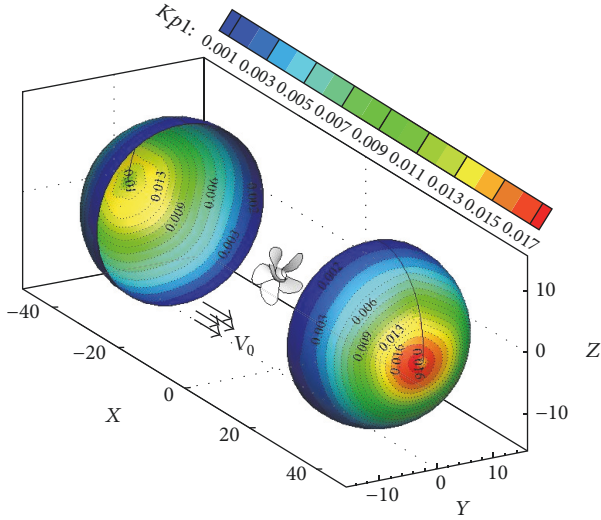
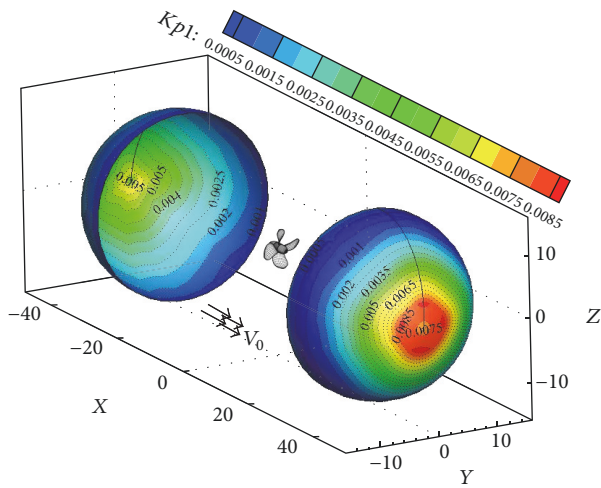Figure 14: 3D contour of single propeller FPF.

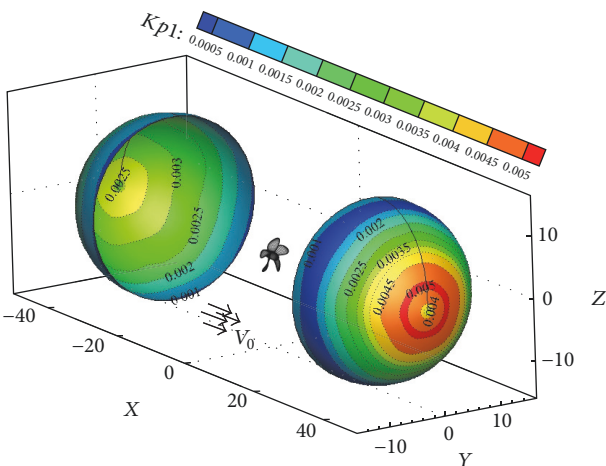Figure 15: 3D contour of front propeller FPF.

Figure 16: 3D contour of rear propeller FPF.

Figures 15 and 16 give the three-dimensional FPFs of the front and rear propellers of CRP. The distribution tendencies of FPFs of the front and rear propellers of CRP are similar to that of the single propeller, the fluctuating pressures downstream are obviously stronger than those upstream, and the weakest fluctuating pressures occur at the propeller rotation plane. The fluctuating pressures of the front and rear propellers of CRP are cyclical, and the cycles have the same numbers of the propeller blades. Compared with the single propeller, the fluctuating pressures induced by the front and rear propellers of CRP are significantly weakened. The first reason is that the load distributions of both the front and rear propellers of CRP are much lower than that of the single propeller with the same thrust being obtained and that the peaks of the fluctuating pressures of the front and rear propellers of CRP are significantly decreased within the slipstream. As the hydrodynamic force amplitudes of the rear propeller are smaller than those of the front propeller, the fluctuating pressure value of the rear propeller is slightly smaller than that of the front propeller. What is more, the interference between the front and rear propellers has an influence on the fluctuating pressure distributions of both propellers. As the rear propeller blades run through the slipstream of the front propeller, the front propeller has a strong influence on the hydrodynamic performance of the rear propeller and makes the inflow velocities of the rear propeller more circumferentially uniform compared with the wake velocities behind the ship hull. Therefore, the pulsation amplitude of unsteady loading on the blade surfaces is smaller, and the FPF of the rear propeller is more uniform and smaller than that of the front propeller.

The total FPFs of CRP are given in Figure 17 in which the fluctuating pressure coefficients are the sums of the fluctuating pressure coefficients of the forward propeller and those of the rear propeller. It can be known from Figures 14 and 17 that the maximum fluctuating pressure of CRP is obviously smaller than that of the single propeller.

In order to have further analysis and better comparison about FPFs between the single propeller and CRP, this paper gives the two-dimensional distribution of the fluctuating pressure of propeller in the longitudinal section in center plane of ship. The positions are given in terms of the angle θ and the distance d. The axial angle θ is measured from the downstream propeller axis and the distance d is $D_s/2$, as shown in Figure 18.

Figure 19 gives the two-dimensional distribution of the fluctuating pressure of the single propeller. The spectra values are plotted as $Kp1$ (first-order fluctuating pressure coefficient) versus position angle, in degree. The single propeller has a strong fluctuating pressure radiation near the hub axis, and local minimum values appear at the hub axis. The fluctuating pressures downstream are obviously greater than that upstream. The weakest fluctuating pressure occurs at the blade rotation plane, and the fluctuating pressure has a strong radiation tendency towards the positions on the hub axis. The resulting fluctuating pressure directivities of the front and rear propellers are shown in Figure 20. The fluctuating pressure directivities of the front and rear propellers have similar tendency to that of single propeller; the fluctuating
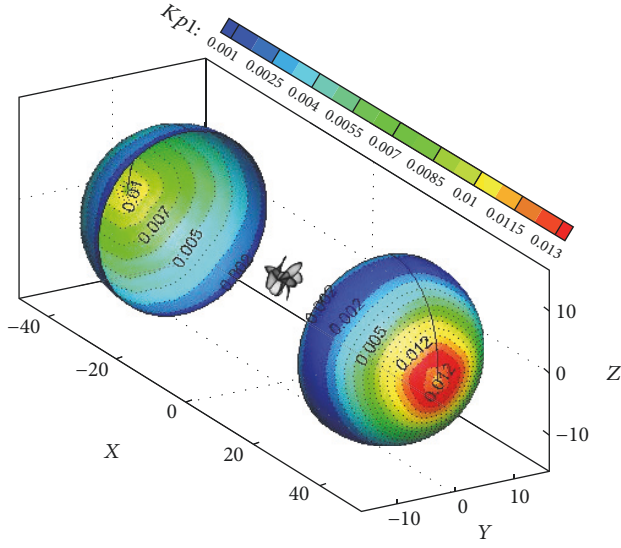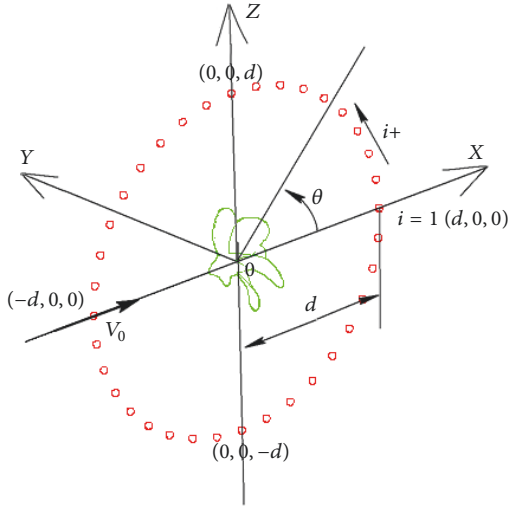
FIGURE 17: 3D contour of the total FPF of CRP.

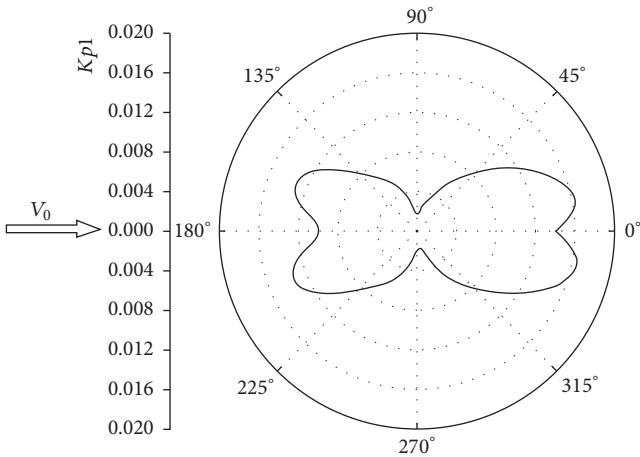FIGURE 18: Schematic of calculation positions.

FIGURE 19: Two-dimensional distribution of the fluctuating pressure of single propeller.
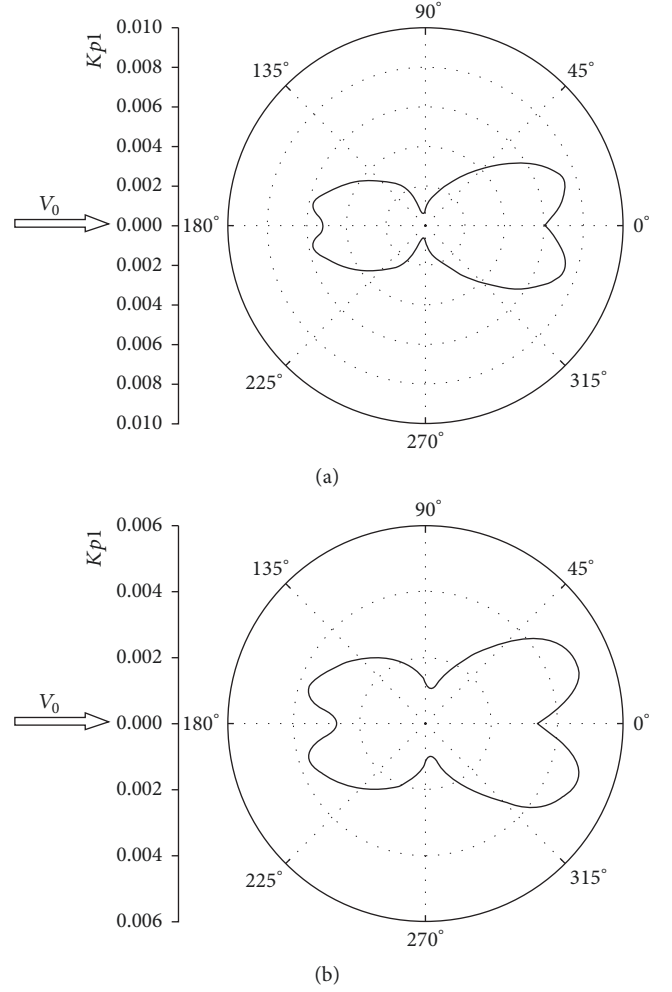

(a)

(b)

FIGURE 20: Two-dimensional distributions of the fluctuating pressures of the forward and rear propellers of CRP. (a) Forward propeller. (b) Rear propeller.

pressures downstream are obviously stronger than those upstream.

In order to have further analysis and better comparison between the FPFs of the single propeller and the CRP system, the overall two-dimensional distribution of the first-order fluctuating pressure of CRP is obtained through superposing the first-order fluctuating pressure of the front and rear propellers, as shown in Figure 21. The fluctuating pressure of the CRP is significantly smaller than that of the single propeller in the upstream as well as at the positions near the hub axis in the downstream. However, the fluctuating pressures of CRP and the single propeller are close near the Y-Z plane in the downstream, and the fluctuating pressure of CRP is even greater than that of the single propeller on the Y-Z plane. It can be known that the CRP and the single propeller have close value of fluctuating pressures in the downstream near the Y-Z plane under the same condition.

5. Conclusions

A theoretical method for the analysis of the fluctuating pressure characteristics of CRP is proposed based on the
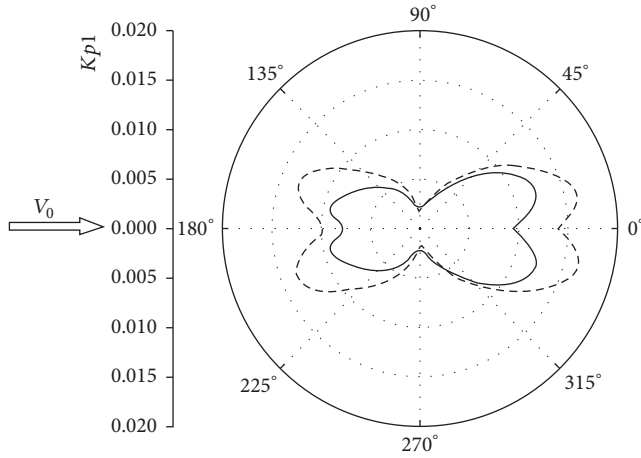
FIGURE 21: Comparison between the overall two-dimensional distribution of the fluctuating pressure of CRP (solid line) and that of single propeller (dash line).

low-order potential based panel method. Through systematic research, the following conclusions can be obtained.

The verification using two given propellers proves the feasibility of the method proposed in this paper. The agreement between the calculation results and the experiment data is excellent. The single propeller has strong fluctuating pressure distribution ahead of the propeller and within the slipstream and may bring serious damage to the vessel hull and the appendages behind the propeller. The FPFs of the front and rear propellers of CRP have similar distribution tendency with the single propeller. The propellers have a strong fluctuating pressure radiation near the hub axis, and local minimum values appear at the hub axis. The fluctuating pressure downstream is greater than that upstream. The weakest fluctuating pressure occurs at the blade rotation planes, and the fluctuating pressure has a strong radiation tendency towards the positions on the hub axis.

Through analysis, the overall fluctuating pressure of CRP is significantly smaller than that of the single propeller in the upstream as well as at the positions near the hub axis in the downstream. The fluctuating pressures of CRP and the single propeller are close near the Y-Z plane in the downstream, and the fluctuating pressure of CRP is even greater than that of the single propeller on the Y-Z plane. Overall, the CRP can improve the stern vibration and cause less damage to the vessel hull as well as appendages behind the thruster.

As the surface panel method adopted in this paper is based on the inviscid flows, the real flow field of single propeller and the CRP cannot be described accurately. Therefore, the calculation results may deviate slightly from the actual situation. The surface panel method will be further improved and more methods as well as model tests will be applied for this topic in the future.

Nomenclature

ρ: Ambient fluid density
ϕ: Velocity potential

φ: Angular position
n: Rotational speed of propeller
D: Diameters of propeller
V_0: Inflow velocity
v_{in}: Induced velocity of propeller
v_t: Total velocity on solid surface
v_d: Induced velocity of solid surface
T: Thrust of propeller
Q: Torque of propeller
$J = V_0/nD$: Advance coefficient of propeller
$K = T/\rho n^2 D^4$: Thrust coefficient of propeller
$K = Q/\rho n^2 D^5$: Torque coefficient of propeller
P_n: nth fluctuating pressure
K_{Pn}: nth fluctuating pressure coefficient
u_g: Amplitude of the wake variation.

Conflicts of Interest

The authors declare that there are no conflicts of interest regarding the publication of this paper.

References

[1] J. P. Breslin, R. J. Van Houten, and J. E. Kerwin, "Theoretical and experimental propeller-induced hull pressures arising from intermittent blade cavitation, loading and thickness," *Transactions-Society of Naval Architects and Marine Engineers*, vol. 90, pp. 111–151, 1982.

[2] Y.-Z. Kehr, C.-Y. Hsin, and Y.-C. Sun, "Calculations of pressure fluctuations on the ship hull induced by intermittently cavitating propellers," *Proceedings of the National Science Council, Republic of China - Part A: Physical Science and Engineering*, vol. 22, no. 5, pp. 642–653, 1998.

[3] H. Seol, "Time domain method for the prediction of pressure fluctuation induced by propeller sheet cavitation: Numerical simulations and experimental validation," *Ocean Engineering*, vol. 72, pp. 287–296, 2013.

[4] S. Berger, M. Baue, and M. Druckenbrod, "An efficient viscous/inviscid coupling method for the prognosis of propeller-induced hull pressure fluctuations," in *Proceedings of 7th International Conference on Ships and Shipping Research*, 2012.

[5] T. T. Kanemaru and J. Ando, "Numerical analysis of pressure fluctuation on ship stern induced by cavitating propeller using a simple surface panel method "SQCM"," in *Proceedings of the 2nd International Symposium on Marine Propulsors*, Hamburg, Germany, 2011.

[6] T. Kawamura and T. Kiyokawa, "Numerical prediction of hull surface pressure fluctuation due to propeller cavitation," in *Proceedings of the Japan Society of Naval Architects and Ocean Engineers*, Nagasaki, Japan, 2008.

[7] K. Sato, A. Oshima, and H. Egashira, "Numerical prediction of cavitation and pressure fluctuation around marine propeller," in *Proceedings of the 7th International Symposium on Cavitation*, 2009.

[8] B. Ji, X. Luo, X. Peng, Y. Wu, and H. Xu, "Numerical analysis of cavitation evolution and excited pressure fluctuation around a propeller in non-uniform wake," *International Journal of Multiphase Flow*, vol. 43, no. 1, pp. 13–21, 2012.

[9] T. Lloyd, G. Vaz, D. Rijpkema, and B. Schuiling, "The potsdam propeller test case in oblique flow: prediction of propeller performance, cavitation patterns and pressure pulses,"

in *Proceedings of the Second Workshop on Cavitating Propeller Performance*, 2015.

[10] P. Peralli, T. Lloyd, and G. Vaz, "Comparison of uRANS and BEM-BEM for propeller pressure pulse prediction: E779A propeller in a cavitation tunnel," in *Proceedings of the 19th Numerical Towing Tank Symposium*, Nantes, France, 2016.

[11] R. E. Bensow and R. Gustafsson, "Effect of propeller tip clearance on hull pressure pulses," in *Proceedings of the 5th International Symposium on Marine Propulsors*, Espoo, Finland, 2017.

[12] D. Ross, *Mechanics of Underwater Noise*, Pergamon Press, Oxford, UK, 1976.

[13] M. Garguet and R. Lepeix, "The problem of influence of solid boundaries on propeller-induced hydrodynamic forces," in *Proceedings of Symposium on High Powered Propulsion of Large Ships*, Wageningen, Netherlands, 1974.

[14] S. Tsakonas, J. P. Breslin, and J. Teeters, *Correlation of Theoretical Predictions of Propeller-Induced Hull Pressures with Available Data*, Stevens Institute of Technology, Hoboken, NJ, USA, 1980.

[15] J. Hu, Y. M. Su, and S. Huang, "Numerical simulation of propeller-induced vibrating pressure on stern," *Journal of Harbin Engineering University*, vol. 26, no. 3, pp. 292–296, 2005.

[16] M. Chen and Q. Zhou, "Numerical simulation of fluctuating propeller forces and comparison with experimental data," *Applied Mechanics and Materials*, vol. 105-107, pp. 518–522, 2012.

[17] E. Güngör and İ. Bedii Özdemir, "Simulation of oblique propeller flow including cavitation and pressure pulses," *Underwater Technology*, vol. 33, no. 4, pp. 203–213, 2016.

[18] M. Osborne, "Design constraints limit options for EEDI compliance," *Naval Architecture*, vol. 25, no. 1, pp. 4–27, 2012.

[19] L. X. Hou, A. K. Hu, and C. H. Wang, "Investigation about the spatial pressure field by the propeller," *Journal of Wuhan University of Technology (Transportation Science Engineering)*, vol. 39, no. 4, pp. 743–746, 2015.

[20] C. Y. Hsin, *Development and analysis of panel methods for propellers in unsteady flow, [Ph.D. thesis]*, Department of Ocean Engineering, Massachusetts Institute of Technology, Cambridge, Mass, USA, 1990.

[21] S. A. Kinnas and N. E. Fine, "A nonlinear boundary element method for the analysis of unsteady propeller sheet cavitation," in *Proceedings of the 19th Symposium on Naval Hydrodynamics*, 1992.

[22] L. Hou, C. Wang, X. Chang, and S. Huang, "Hydrodynamic performance analysis of propeller-rudder system with the rudder parameters changing," *Journal of Marine Science and Application*, vol. 12, no. 4, pp. 406–412, 2013.

Journal of
Engineering

The Scientific
World Journal

International Journal of
Rotating
Machinery

Journal of
Sensors

Advances in
Multimedia

Advances in
Civil Engineering

Journal of
Control Science
and Engineering

Journal of
Robotics

Journal of
Electrical and Computer
Engineering

Advances in
OptoElectronics

VLSI Design

International Journal of
Navigation and
Observation

Modelling &
Simulation
in Engineering

International Journal of
Aerospace
Engineering

International Journal of
Chemical Engineering

International Journal of
Antennas and
Propagation

Active and Passive
Electronic Components

Shock and Vibration

Advances in
Acoustics and Vibration

Hindawi

Submit your manuscripts at
www.hindawi.com